COMBINING MULTIPLE SOURCES FOR RADIOMETRIC CALIBRATION OF LANDSAT 7 USING A KALMAN FILTER

Ellis Freedman and Jennifer Byrne
Martin Marietta Corporation
Management and Data Systems
P.O. Box 8555
Philadelphia, Pennsylvania U.S.A 19101
Telephone: (610) 531-1684
Fax: (610) 962-3698
E-Mail: freedmae@land.vf.ge.com

KEY WORDS: Kalman Filter, Radiometry, Calibration, Landsat 7

ABSTRACT

The Enhanced Thematic Mapper Plus, currently under development for Landsat 7, has a requirement to provide absolute radiometric information with errors of less than 5%. To meet this requirement, current plans call for the use of three different techniques for absolute radiometric calibration: Full Aperture Solar Calibration, Partial Aperture Solar Calibration, and Ground Look Calibration. Associated with each of these is its own set of uncertainties and errors which may, at times, exceed the system's allowable error margin. A Kalman Filter is proposed for combining the outputs of all three techniques, and for the optimal estimation and continual updating and tracking of the states of the associated hardware calibrators. Results are presented which surpass the requirement and indicate the viability of the approach.

1. INTRODUCTION

The Thematic Mappers (TM) of Landsat 4 and 5 had goals of achieving less than 10% error in absolute radiometric accuracy. To achieve this goal, the TMs were calibrated in the laboratory using equipment that had an estimated radiometric uncertainty of approximately 10%. Once on-orbit, the calibration coefficients were updated with an internal calibrator that provided both a dark shutter and various levels of light. While no definitive evaluation of performance is available, different studies indicate that as much as 10% – 15% additional drift may have occurred since launch.

Landsat 7 will take a different approach. The Enhanced Thematic Mapper Plus (ETM+), while similar in its core design to the TM, will include not only an internal calibrator similar to that on the TM, but two additional radiometric calibration devices: the Full Aperture Solar Calibrator (FASC) and the Partial Aperture Solar Calibrator (PASC). Briefly, the FASC is a paddle that can be positioned in front of the ETM+ aperture covering the entire field of view. On the surface of the paddle facing the aperture is a panel of highly reflective, highly diffuse (nearly Lambertian), YB-71 white thermal control paint. The paddle is positioned during calibration in such a way as to reflect sunlight into the field of view providing a well-characterized source of radiance. Calibration is scheduled to take place approximately once every six weeks when the satellite passes over the (North Pole) terminator.

The PASC is a completely different form of calibrator. It will consist of a small device in four parts which sits inside the sunshade. Each part will be made up of two reflecting surfaces and a small aperture. Approximately when the satellite passes over the North Pole and the Earth below is in darkness, sunlight will be reflected sequentially off the two surfaces and through the small aperture enabling the ETM+ to effectively create an image of the Sun through a combination of the whiskbroom scanning in one direction and the relative satellite motion in the other. This apparatus is duplicated four times to account for angular variations of Sun position with season (i.e. the Sun will be seen through different apertures at different times of the year). Current plans call for the PASC to be used once a day.

The combination of all three techniques will provide a large amount of data on the radiometric response of the ETM+. However, each technique will have its own characteristic uncertainties, and questions quickly arise over how much the data from each form of calibration should be trusted and how the data should be combined to estimate the response of the sensor. Proper estimation of the errors and characteristics of each technique in combination with an optimal estimator, such as a Kalman Filter, can provide a better understanding of the sensor response than any single calibration technique might provide. This paper provides a description of some of the work done in developing that Kalman Filter. All work presented here is presumed to apply to band one (0.45μm – 0.515 μm) of the ETM+, although it is directly applicable to all of the other reflective bands (2 – 5, 7 and the new Panchromatic band).

2. THE KALMAN FILTER

A Kalman Filter is, in simple terms, a linear estimator/predictor which provides an optimized estimate of a set of measured parameters (the state vector) given certain characteristics about the system being measured and the measuring device.

Developing the filter requires a degree of knowledge of the random error associated with the measuring device for each parameter to be estimated (the measurement noise), a similar knowledge of the randomness in the parameter being measured (the process noise), and a model of how the parameters change from one state to the next (the transition operation). In the basic Kalman Filter, noise is assumed to be white and Gaussian. From this information (which is never perfectly known), the filter will dynamically determine, with each new measurement, the weight (i.e. trust) that should be placed on each new measurement versus that of its own internal model/prediction. The first step in developing a Kalman Filter is, therefore, to characterize the system. Development of the filter after that step is relatively straightforward. Finally, the filter must be tested in a simulation which models a true world, which differs from that assumed by the filter, in order to evaluate its ability to adapt to unknowns and still determine the correct state of the system.

3. CHARACTERIZATION OF DIFFERENT CALIBRATION TECHNIQUES

In addition to calibrating with the FASC and PASC, plans also call for performing Ground Look Calibration (GLC). In that case a ground truth team will be located at a prearranged site taking a variety of readings of surface radiance and reflectivity and atmospheric conditions while ETM+ images the scene. Calculations will be performed on the ground truth data to determine the effective radiance seen by the sensor at the top of the atmosphere. GLC will be nominally scheduled once every two to six months after initial on-orbit calibration.

Based upon estimates from Santa Barbara Research Center (SBRC), the developer of the ETM+ and its solar calibrators, the FASC will initially have two error sources which, when combined, will provide a total of 3.2%(1σ) radiometric error: uncertainties in the measured Bidirectional Reflectance Distribution Function (BRDF), and geometric alignment errors. Approximately 1.5% (1σ) radiometric error is due to the randomness in positioning the FASC in the field of view with each calibration. Thus it varies with time. The remainder of the total can be considered an initial bias error. As a conservative measure, the larger values of 4.4% and 1.7% were chosen to represent the true initial and random errors.

In addition to the initial bias error and a random component over time, it is also known that the effective reflectivity of YB-71 is altered with exposure to UV, atomic oxygen, and contamination. The degree and rate of this change is, however, open to debate. Results from the LDEF satellite (Bruegge, 1991), as well as from various laboratories differ in magnitude, and generally do not represent the conditions expected for Landsat 7. Therefore, a worst case condition was chosen to represent the simulated true band 1 degradation (the most sensitive band) in effective reflectivity of 22% over 5 years.

Also based upon SBRC estimates, the PASC was assumed to have a small degradation in its effective throughput (transmission) of 5% over 5 years due to the effects of contamination. The random component was assumed to be very small, due to a lack of random contributors. However, because of contamination problems encountered with early Landsat vehicles with similar devices, to be conservative, a true initial error of 10% was assumed.

Estimation of the accuracy of exoatmospheric radiometry using ground truth and atmospheric modeling is somewhat subjective due to the dependence on the type of modeling, and the type and precision of the ground truth collected. No decision has yet been made about the source for such measurements. However, based upon estimates from other studies, both in-house and external (Green, 1994 and Hartmann, 1983), a true constant bias error of 5% and a time-varying random error of 2.5% (1σ) with no long term drift was assumed.

Collections were assumed to take place at the following intervals:

1. FASC at days 16, 24, 32, 40, and 48 days after launch and every 45 days thereafter.
2. PASC every day after launch starting with day 16.
3. GLC at days 16, 32, and 48 days after launch and every 90 days thereafter.

4. TRUTH MODEL

The truth model was developed based on engineering insight, experience, and analysis of "worst case" conditions. It served as the basis for evaluating the potential for achieving the desired absolute radiometric accuracy in the face of anticipated uncertainty in the dynamics and measurement models incorporated into the Kalman Filter. The variables estimated at each time step, i.e., the state variables, were the reflectivity of the FASC paddle as a function of time, ϱ, and the effective throughput of the PASC optics as a function of time, τ. The true value of these quantities change dynamically and are not known exactly, even at the initial time step. To simulate the true dynamics, however, the following equations were used.

$$\varrho_{true}(t) = \frac{24.154589}{t + 120.77295} + 0.7 + e_{F,true}(t) \qquad (1)$$

$$\tau_{true}(t) = \tau_{0,true} \exp(-\alpha_{true} t) + e_{P,true}(t) \quad (2)$$

where $e_{F,true}$ is a random variable with zero mean and standard deviation of $\varepsilon_{F,true}$, and $e_{P,true}$ is a random variable with zero mean and standard deviation of $\varepsilon_{P,true}$ (see Table 1).

The gain of the detector also was assumed to change with time, but it was not one of the state variables in this Kalman Filter. The following equation, based on analysis of data from the detectors in band 1 of the Thematic Mapper sensor on Landsat 5, was used to describe how the gain of the detectors in band 1 changed as a function of time:

$$G(t_{k+1}) = G(t_k) - 0.0000444227 + e_{gain} \quad \text{with} \quad G(t_0) = 1 \quad (3)$$

where e_{gain} is a random variable with zero mean and standard deviation of ξ_P (see Table 1). The data generated using Equations (1) through (3) was used to evaluate the output of the Kalman Filter, as well as to provide input to the Kalman Filter in the form of simulated measurements.

The truth model provided simulated FASC, PASC, and GLC measurements (D_F, D_P, and D_G output detector counts) to the filter, at the frequency specified in Section 3 of this paper, using the following equations:

$$D_G(t_k) = G(t_k) R_G(t_k) \quad (4)$$

$$D_F(t_k) = G(t_k) \varrho_{true}(t_k) R_{SF}(t_k) \quad (5)$$

$$D_P(t_k) = G(t_k) \tau_{true}(t_k) R_{SP}(t_k) \quad (6)$$

where ϱ and τ were as specified in Equations (1) and (2), G was as specified in equation (3) and R_G, R_{SF}, and R_{SP}, the true GLC radiance, true full aperture solar radiance, and true partial aperture solar radiance, were computed using the following equations:

$$R_G(t_k) = \overline{R}_G + e_G(t_k) \quad (7)$$

$$R_{SF}(t_k) = \overline{R}_{SF} + e_{SF}(t_k) \quad (8)$$

$$R_{SP}(t_k) = \overline{R}_{SP} + e_{SP}(t_k) \quad (9)$$

In equations (7) through (9), e_G, e_{SF}, and e_{SP} are random variables with zero means and standard deviations of $\varepsilon_{G,true}$, $\varepsilon_{SF,true}$, and $\varepsilon_{SP,true}$, respectively (see Table 1), and "barred" variables are mean radiance values.

PARAMETER	TRUE	MODELED
ϱ (INITIAL)	0.9	0.86
τ (INITIAL)	0.06	0.054
ε_{SF} (solar variability for FASC)	0.18%	0.18%
ε_{SP} (solar variability for PASC)	0.18%	0.18%
ε_F (randomness in FASC)	1.7%	1.7%
ε_P (randomness in PASC)	0.02%	0.02%
ε_G (randomness in true GLC radiance)	0.0%	0.0%
ξ_F (detector gain drift at FASC)	0.2%	0.2%
ξ_P (detector gain drift at PASC)	0.2%	0.2%
η_G (randomness in modeled GLC input radiance)	2.5%	2.5%
β_G (bias in GLC radiance)	5.0%	0.0% (estimated from data)
α	0.000028*	0.0001**
b	Asymptotic***	0.0000577****

Table 1. Initial Values and Noise Statistics Assumed for Kalman Filter and Truth Model

* Represents 5% degradation in partial aperture over 5 years.
** Represents 17% degradation in partial aperture over 5 years.
*** Represents 22% degradation in full aperture over 5 years (with rapid degradation in first year).
**** Represents <1% degradation in full aperture over 5 years.

In addition to the simulated measurements, estimates of the GLC radiance (R_G), Solar Radiance at the Full Aperture (R_{SF}), and Solar Radiance at the Partial Aperture (R_{SP}) were also provided to the Kalman Filter. During the mission, these estimates will be obtained using ground truth teams (R_G) and solar and atmospheric models (R_{SF} and R_{SP}). The estimates were simulated using the following equations:

$$R^*_G(t_k) = \overline{R}_G + \beta_{G,true} + n_G(t_k) \tag{10}$$

$$R^*_{SF}(t_k) = \overline{R}_{SF} + \beta_{SF,true} \tag{11}$$

$$R^*_{SP}(t_k) = \overline{R}_{SP} + \beta_{SP,true} \tag{12}$$

where n_G is a random variable with zero mean and standard deviation of $\eta_{G,true}$ (see Table 1); $\beta_{G,true}$, $\beta_{SF,true}$, and $\beta_{SP,true}$ (see Table 1) are biases associated with the algorithms used to estimate the GLC radiance, partial aperture solar radiance, and full aperture solar radiance, respectively; and the asterisk denotes the simulated estimate.

5. KALMAN FILTER INTERNAL MODELS

There were two mathematical models inherently embodied in the Kalman Filter: a model which described how the state variables, ϱ and τ, were expected to change with time (the state dynamics model), and a model which described how the measurements at a given time step (D_G, D_F, and D_P) were expected to relate to the state variables at that time step (the measurement model). Although several Extended Kalman Filter formulations have been investigated during this work, the discussion in this paper will be limited to the static, linear Kalman Filter which has the form:

$$\mathbf{x}_{k+1} = \phi\mathbf{x}_k + \mathbf{w}_k \tag{13}$$

$$\mathbf{z}_k = \mathbf{H}\mathbf{x}_k + \mathbf{v}_k \tag{14}$$

where $\mathbf{x}$ is the state vector consisting of ϱ and τ, ϕ is the state transition matrix, $\mathbf{w}$ is the dynamics noise vector with strength $\mathcal{E}\{\mathbf{w}\mathbf{w}^T\} = \mathbf{Q}_k\delta_k$, $\mathbf{z}$ is the measurement vector, $\mathbf{H}$ is the matrix which relates the states to the measurements, and $\mathbf{v}$ is the measurement noise vector with strength $\mathcal{E}\{\mathbf{v}\mathbf{v}^T\} = \mathbf{R}_k\delta_k$.

The models of the form of Equations (13) and (14) were developed based on the truth model. However, the truth model was developed based on limited information. Thus, it was necessary to investigate the sensitivity of the candidate Kalman Filter to knowledge of the true parameters. For this reason, the parameters and internal models of the Kalman Filter intentionally deviated from the parameters and models in the truth model. The state dynamics model was represented by:

$$\varrho_{k+1} = \exp(-b_{model}t_k)\varrho_k + e_{F,model} \tag{15}$$

$$\tau_{k+1} = \exp(-\alpha_{model}t_k)\tau_k + e_{P,model} \tag{16}$$

where b_{model} and α_{model} are given in Table 1, $e_{F,model}$ is a random variable with zero mean and standard deviation of $\varepsilon_{F,model}$ (see Table 1), and $e_{P,model}$ is a random variable with zero mean and standard deviation of $\varepsilon_{P,model}$ (see Table 1).

Note the difference between the true representation of the state dynamics, Equations (1) and (2), and the Kalman Filter representation, Equations (15) and (16). Due to the uncertainty associated with the parameters b_{model} and α_{model}, parameter estimation was sometimes performed on the filter outputs, i.e., the estimates of ϱ and τ, to successively refine the estimates of b_{model} and α_{model}.

The measurement model has two components which together comprise the form of Equation (14):

$$H_k = \begin{bmatrix} \frac{D_{G,k}}{R^*_{G,k}} R^*_{SF,k} & 0 \\ 0 & \frac{D_{G,k}}{R^*_{G,k}} R^*_{SP,k} \end{bmatrix} \quad (17)$$

$$R_k = \begin{bmatrix} \sigma^2_{D_{F,k}} & \sigma_{D_{F,k}} \sigma_{D_{P,k}} \\ \sigma_{D_{P,k}} \sigma_{D_{F,k}} & \sigma^2_{D_{P,k}} \end{bmatrix} \quad (18)$$

In equation (18), $\sigma^2_{DF,k}$, $\sigma_{DF,k}\sigma_{DP,k}$, $\sigma_{DP,k}\sigma_{DF,k}$, and $\sigma^2_{DP,k}$ are functions of the ground truth measurements, the state variables at the previous time step, and random variables with zero means and standard deviations of $\varepsilon_{G,model}$, $\varepsilon_{SF,model}$, $\varepsilon_{SP,model}$, $\xi_{FG,model}$ $\xi_{PG,model}$, and $\eta_{G,model}$ (see Table 1).

One last item of extreme importance was the initial procedure for "removing" bias errors in the estimated GLC radiance. During the first 48 days following (simulated) launch, it was assumed that the modeled radiance from the FASC was effectively correct (i.e. that the FASC had not yet begun to decay). The average difference between the first three GLC radiances and the corresponding FASC radiances was removed as a bias term in all of the GLC radiance estimates, thus providing an initial anchor, albeit an errored one, to a better estimate of the true radiance.

Table 1 contains the parameters used for simulations discussed in this paper. Simulations were also conducted for a wide variety of other "truth" conditions, as part of a sensitivity analysis. Again, since the actual state dynamics process will not be characterized, the underlying Kalman Filter must be robust enough to provide satisfactory results with limited knowledge of the true system dynamics.

The following section discusses the results obtained using the basic Kalman Filter under the conditions represented in Table 1.

6. SIMULATION RESULTS

Figure 1 presents six graphs of the results of one simulated run which used one random seed out of the twenty attempted. All of the graphs show results over time in units of days since launch. Graphs a, c, and e compare the true variation versus the variation estimated by the model for the FASC effective reflectivity (ϱ), the PASC effective throughput (τ), and the gain of a detector, respectively. In the case of ϱ and ϱ_{true}, the curves overlap so that they are indistinguishable, although the random variability might appear to be greater than expected. Yet, at least superficially, the filter appears to be tracking the variation in the reflectivity.

In the case of throughput, since the random component is smaller, it is easier to see the fidelity with which the filter tracks the actual variations. Here it is quite obvious that the filter is closely tracking reality.

	−5% error in ϱ_0 −5% GL bias 2.5% GL random		−5% error in ϱ_0 −5% GL bias 5% GL random		−5% error in ϱ_0 5% GL bias 2.5% GL random		−5% error in ϱ_0 5% GL bias 5% GL random		5% error in ϱ_0 −5% GL bias 2.5% GL random		5% error in ϱ_0 −5% GL bias 5% GL random		5% error in ϱ_0 5% GL bias 2.5% GL random		5% error in ϱ_0 5% GL bias 5% GL random	
	μ	σ	μ	σ	μ	σ	μ	σ	μ	σ	μ	σ	μ	σ	μ	σ
A	−1.84	1.69	−2.03	2.23	2.73	1.39	1.02	1.9	−3.3	1.65	−1.86	2.07	−1.32	1.49	0.65	1.92
B	−3.06	1.66	−3.26	2.22	−0.53	1.45	1.02	1.9	−0.98	1.47	−5.84	2.27	−5.52	1.67	−5.84	2.27
C	−1.92	1.77	3.7	2.0	−0.55	1.5	0.75	1.96	−3.4	1.72	−2.01	2.16	−1.34	1.53	0.44	1.97
D	−3.21	1.71	3.7	1.9	−0.55	1.5	0.74	1.96	−3.4	1.73	−5.99	2.35	−5.55	1.71	−1.55	2.08

Model Descriptions

A:	ϱ	asymptotic	C:	ϱ	asymptotic
	τ	exponential		τ	asymptotic
B:	ϱ	exponential	D:	ϱ	exponential
	τ	exponential		τ	asymptotic

Table 2. Results of Monte Carlo Analysis

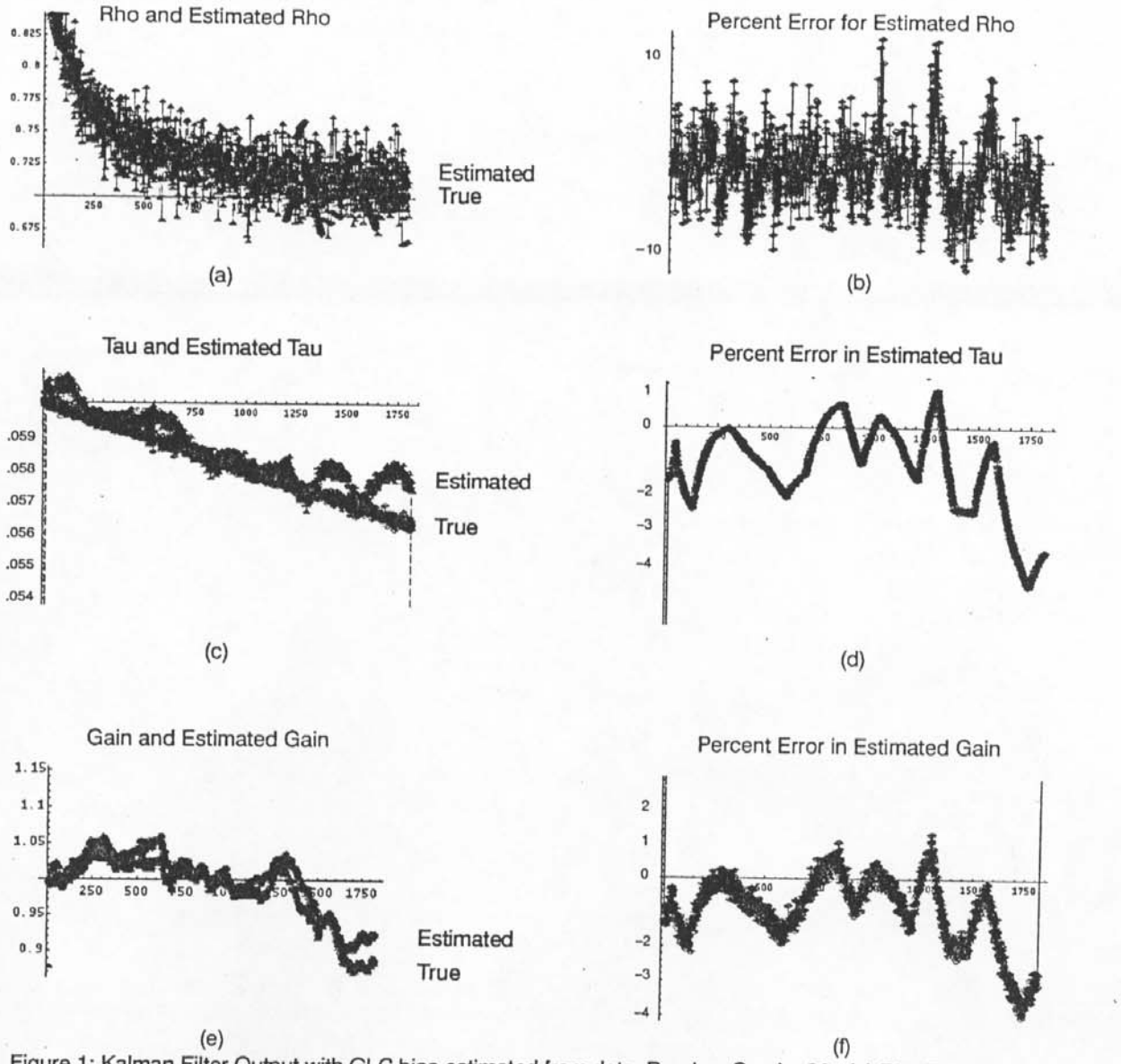

Figure 1: Kalman Filter Output with GLC bias estimated from data, Random Seed = 29. (a) Rho Estimate and Rho True. (b) Percent Error in Rho Estimate. (c) Tau Estimate and Tau True. (d) Percent Error in Tau Estimate. (e) Gain and Estimated Gain. (f) Percent Error in Estimated Gain.

Graph e presents the most important result, the comparison of estimated detector gain and actual detector gain. It is clearly evident that, despite initially large errors in the PASC, and errors which rise dramatically in the FASC, the filter has managed to closely track (usually within 3%), and therefore enable the calibration of the detector.

Graphs b, d, and f present the percentage differences between the curves in a, c, and e, respectively.

A series of several hundred simulated Monte Carlo runs (see Table 2.) indicated that the filters are relatively insensitive to errors in estimating the magnitude of the noise (measurement and process) statistics. In Table 2., the mean and standard deviation over one hundred sample runs of the detector gain error is presented for various combinations of initial FASC reflectivity error, exoatmospheric ground look radiance bias and random errors, and assumed FASC and PASC degradation modeling characteristics. Where the model is labeled as asymptotic, the characteristic was assumed to have degraded inversely with time, as in equation (1), and where it is labeled as exponential, the modeled degradation takes the exponential form of equations (15) and (16). In most cases, the residual mean/bias error is well below the 5% goal, and in all cases, the random is less than 2.3%. Also, although not detailed here, tripling the estimates of the noise caused no significant changes in either the settling time or residual error magnitude. The filters were also insensitive to the degradation model assumed for the FASC, primarily because of its infrequent measurements. All of the filters stabilized quickly. The 5% error limit goal was usually reached within 48 simulated days of launch, with quantitative indications of stability occurring within 150 days.

Subsequent analyses indicated that most of the residual error was in the form of a bias error resulting from the small number of sample points (3) used to initially remove the bias between the GLC and the FASC. Statistical evaluations have shown that increasing the number of sample points to as little as five would effectively eliminate the bulk of this residual.

One final analysis performed was the non–linear least squares curve fit of the state vector estimates of the Kalman Filter to the internal models of behavior after a simulated 2.5 years and 5 years on–orbit. Both sets of results indicate that RMS errors were reduced to less than 1%. Therefore, while not providing "real time" improvements, a posteriori back filtering seems to have the potential to further improve radiometric estimates of historical data.

7. CONCLUSIONS

Although additional Monte Carlo computer runs could be made in order to provide a more statistically significant sample set, these initial runs do provide evidence that a relatively simple Kalman Filter can synergistically combine information from different types of radiometric calibrators both to track and compensate for variations in the sensor and calibrators, and minimize residual errors. The key to success is a combination of sources with complementary strengths (initial accuracy for the FASC, frequent updates and low randomness for the PASC, no drift in the GLC) which can be correlated through the Kalman Filter. In this case, the FASC and PASC were correlated through the detector gain determined from the GLC. The results are, of course, highly dependent upon the assumptions made in the study. The strongest sensitivity seems to be to the random error in the estimated exoatmospheric GLC radiance and the degree to which it will hamper determination of the bias error. (Note: Randomness in the exoatmospheric GLC radiance is not the variability in the radiance, which is constantly changing, but in the error about the true value.) It is believed that such randomness can be minimized through the judicious selection of a high, dry, ground calibration target.

Additionally, such a technique may be applicable to other radiometric remote sensing platforms with multiple calibration sources. Several multispectral remote sensing platforms are planned for the next decade, and most of them will employ several radiometric calibrators. In many cases, a technique for combining the different calibration results has not yet been determined. This approach may provide one possible method for their combination.

8. ACKNOWLEDGEMENTS

This work was performed in support of NASA contract NAS532633.

The authors also wish to gratefully acknowledge the support of the engineers and scientists at Santa Barbara Research Center, the Landsat Program Office at Goddard Space Flight Center, and the EROS Data Center, without whose help this work would not have been possible.

9. REFERENCES

Bruegge, C. J. and Stiegman, A., October 2, 1991. Memo to Bruce Guenther at Jet Propulsion Laboratory on Spectralon Diffuse Panel.

Green, R. O., June 17, 1994. Status letter on AVIRIS activities at Jet Propulsion Laboratory.

Hartmann, D. L., November 1983. Total Solar Irradiance Monitoring, Report of the Atmospheres Panel to the Payload Panel. The Earth Observer, pp. 23–27.

Malinowski, F., 28 May, 1993. AI #49 – Provide GE with Long Term Signal and Noise Data for L5. Santa Barbara Research Center, Internal Memorandum PL2807L–T00761.

Olsson, H., June 1993. Recent Absolute Radiometric Calibration of Landsat–5 TM and Its Application to the Atmospheric Correction of ASTER in the Solar Reflective Region, Workshop on Atmospheric Correction of Landsat Imagery, pp. 167–171.

Thome, K. J., Biggar, S.F., and Slater, P.N., June 1993. Recent Absolute Radiometric Calibration of Landsat–5 TM and Its Application to the Atmospheric Correction of ASTER in the Solar Reflective Region. Workshop on Atmospheric Correction of Landsat Imagery, pp. 36–40.